Fructose-derived advanced glycation end-products drive lipogenesis and skeletal muscle reprogramming via SREBP-1c dysregulation in mice

Fructose-derived advanced glycation end-products drive lipogenesis and skeletal muscle reprogramming via SREBP-1c dysregulation in mice.

Mastrocola R[1], Nigro D[1], Chiazza F[2], Medana C[3], Dal Bello F[3], Boccuzzi G[4], Collino M[2], Aragno M[1].

[1]Department of Clinical and Biological Sciences, University of Turin, Italy; [2]Department of Drug Science and Technology, University of Turin, Italy; [3]Department of Molecular Biotechnology and Health Sciences, University of Turin, Italy; [4]Department of Medical Sciences, University of Turin, Italy.

Running title: Fructose-derived AGEs and SREBP1c dysregulation

Corresponding author:

Raffaella Mastrocola
Department of Clinical and Biological Sciences,
University of Turin
Corso Raffaello 30
10125 Turin, Italy.
Tel. +39 011 6707758
Fax +39 011 6707753
e-mail address: raffaella.mastrocola@unito.it

List of abbreviations: ACC, acetyl-Coenzyme A carboxylase; AGE-R1, AGE receptor-1; AGEs, advanced glycation end-products; CML, carboxy-methyllysine; CPT-1m, carnitine palmytoiltransferase-1 muscle; FASN, fatty acid synthase; IMCL, intramyocellular lipids; MEF2c, myocyte enhancer factor 2c; MHC, myosin heavy chain; MnSOD, manganese superoxide dismutase; MRFs, myogenic regulatory factors; MyoD1, myogenic differentiation 1; RAGE, receptor for advanced glycation end products; ROS, reactive oxygen species; SCAP, SREBP cleavage-activating protein; SDH, succinic dehydrogenase; SIRT-1, sirtuin-1; sMtCK, sarcomeric mitochondrial creatine kinase; SREBP-1c, sterol regulatory element-binding protein-1c.

Abstract

Advanced Glycation End-Products (AGEs) have been recently related to the onset of metabolic diseases and related complications. Moreover, recent findings indicate that AGEs can endogenously be formed by high dietary sugars, in particular by fructose which is widely used as added sweetener in foods and drinks. The aim of the present study was to investigate the impact of a high-fructose diet and the causal role of fructose-derived AGEs in mice skeletal muscle morphology and metabolism. C57Bl/6J mice were fed a standard diet (SD) or a 60% fructose diet (HFRT) for 12 weeks. Two subgroups of SD and HFRT mice received the anti-glycative compound pyridoxamine (150 mg/kg/day) in the drinking water. At the end of protocol high levels of AGEs were detected in both plasma and gastrocnemius muscle of HFRT mice associated to impaired expression of AGE-detoxifying AGE-receptor 1. In gastrocnemius, AGEs upregulated the lipogenesis by multiple interference on SREBP-1c through downregulation of the SREBP-inihibiting enzyme SIRT-1 and increased glycation of the SREBP-activating protein SCAP. The AGEs-induced SREBP-1c activation affected the expression of myogenic regulatory factors leading to alterations in fiber type composition, associated with reduced mitochondrial efficiency and muscular strength. Interestingly, pyridoxamine inhibited AGEs generation, thus counteracting all the fructose-induced alterations. The unsuspected involvement of diet-derived AGEs in muscle metabolic derangements and proteins reprogramming opens new perspectives in pathogenic mechanisms of metabolic diseases.

Key words: Fructose; AGEs; carboxy methyllysine; SREBP-1c; lipogenesis; myogenic regulatory factors; mitochondrial oxidation; muscle strength; pyridoxamine.

Introduction.

Fructose is often used as added sweetener in foods and beverages for both its supposed healthy effects when in the pure form and its low cost when used in the form of high-fructose corn syrup [1,2]. However, the increased consumption of fructose occurred in the last decades has been related to the worldwide rise in diabetes, insulin-resistance, obesity, and other metabolic diseases [3-5]. We have recently demonstrated that, besides its well-known lipogenic effect, chronic fructose exposure in mice generates advanced glycation end-products (AGEs) in plasma and liver at higher level than glucose [6].

AGEs are reactive compounds deriving from glycoxidation reactions between the amino group of proteins and reducing sugars [7], among which one of the most studied is carboxy-methyllysine (CML). AGEs are well known for their role in diabetes complications development, as they are generated during chronic hyperglyceamia [8]. However, a growing body of evidence has shown that AGEs can also be introduced with foods as a result of cooking and heating [9], but also an excessive sugar intake is supposed to be a source of endogenous AGEs [10,11].

As for fructose, also for dietary AGEs a role in the onset of obesity and lipids accumulation, as well as in insulin-resistance has been reported [12-14]. In particular, CML is reported to be increased in fatty livers and in skeletal muscle of obese patients [15,16]. Conversely, the restriction of dietary AGEs has been found to lower insulin levels, markers of insulin resistance, and inflammation [17] and the inhibition of AGEs by pyridoxamine was able to improve obesity and skeletal muscle glucose uptake in mice fed a high-fat diet [18]. Pyridoxamine is a vitamin B6 metabolite which has been proved to be a potent quencher of the dicarbonyl compounds precursors of the AGEs in both *in vitro* and in animals studies [19,20]. Its anti-glycative action is strengthen by metal ions chelation [21] and reactive species neutralization [19] abilities. However, the clinical evidence on the potential AGEs-inhibiting effects of pyridoxamine is still limited and there are several ongoing human trials on different AGEs-related diseases [22,23].

Nevertheless, the mechanisms by which AGEs mediate metabolic changes are poorly understood and the range of effects of fructose-derived AGEs on tissue metabolism is far from being fully explored. Three mechanisms have been proposed by which AGEs could interfere with cell functions: (i) accumulation of AGEs in the extracellular matrix; (ii) binding of AGEs to AGE-receptors, such as the receptor for advanced glycation end products (RAGE), leading to activation of pro-inflammatory signaling; (iii) intracellular AGEs formation [22]. On the other hand, the deleterious effects of AGEs may be counteracted by the binding of AGEs with the AGE receptor-1 (AGE-R1), which both induces AGEs degradation and blocks RAGE-mediated pro-inflammatory signaling [24].

Notably, very little is known about the effects of AGEs in skeletal muscle. The accumulation of AGEs has been suggested to affect skeletal muscle function during ageing and to contribute to intramyocellular lipid accumulation in obesity [16,25].Very recently we have documented that AGEs accumulate in gastrocnemius muscle in obese mice and that this accumulation is associated to activation of the SCAP/SREBP lipogenetic pathway that, in turn, triggers lipids production and accumulation [26]. Here we further extend our previous observations investigating whether mice skeletal muscle structure and metabolism can be affected by chronic exposure to a high-fructose diet and we better characterize the causal role of fructose-derived AGEs by using the glycation inhibitor pyridoxamine.

Materials and methods.

Animals and treatments

Male C57Bl/6j mice (Charles River Laboratories, Calco, Italy) aged 4 weeks were cared for in compliance with the European Council directives (No. 86/609/EEC) and with the Principles of Laboratory Animal Care (NIH No. 85–23, revised 1985). The scientific project was approved by the Ethical Committee of the Turin University (permit number: D.M. 94/2012-B). Mice were fed a standard diet (SD group, $n = 14$) providing 70% of calories in carbohydrates (55% from corn starch

and 15% from maltodextrin), or a 60% fructose diet (HFRT group, *n* = 24) providing 70% of calories in carbohydrates (10% from corn starch and 60% from fructose), for twelve weeks. After three weeks of dietary intervention, during which body weight, glycemia, and food and water intake were strictly monitored, two subgroups of SD and HFRT diet started pyridoxamine supplementation in the drinking water for the remaining nine weeks (SD+P, *n* = 6; HFRT+P, *n* = 12). The pyridoxamine dosage (1 g/L, the equivalent of about 150 mg/kg bw/day) was chosen according to literature data [27] and calculated on the average daily water intake. All groups received drink and food *ad libitum*.

Limb muscle strength tests

After 12 weeks of dietary manipulation muscle strength performances were assessed. Kondziela's inverted screen test was performed as shown and described by Deacon [28]. Resistance to fatigue was expressed as minutes after which the mouse falls off the inverted screen, with a maximum criterion time of 20 minutes.

Grip test was performed as described by MacArthur, et al. [29] using a homemade grip strength-meter. Each mouse was allowed to grasp the trapeze with their forelimbs and then pulled slowly backward. The mouse released the bar at its peak strength and this tension was measured by the dynamometer in Newtons. This process was repeated three times for each mouse and the results averaged as the grip strength for that animal.

Procedures and plasma analyses

Body weight and drink/food intake were recorded weekly. Six-hours fasting glycemia was measured at the start of the protocol and every 4 weeks by saphenous vein puncture using a conventional glucometer. After 12 weeks, mice were anesthetized and killed by cardiac exsanguination. Blood was collected and the gastrocnemii were rapidly removed.

The right gastrocnemius was cryoprotected in Optimal Cutting Temperature compound and frozen in liquid N_2 for cryostatic preparations. The left gastrocnemius was frozen in liquid N_2 and stored at −80°C for protein analysis. Plasma lipid profile was determined by standard enzymatic procedures

using reagent kits. Plasma insulin level was measured using an enzyme-linked immunosorbent assay (ELISA) kit.

Gastrocnemius lipid content

For tissue triglyceride (TG) content determination, colorimetric assay kit was used after lipid extraction. Gastrocnemius intramyocellular lipid (IMCL) accumulation was evaluated by Oil Red staining on 10 μm cryostatic sections.

Preparation of tissue extracts

Gastrocnemius total proteins were extracted as previously described [26] from 10% (w/v) gastrocnemius homogenates in RIPA buffer (0.5% Nonidet P-40, 0.5% sodium deoxycholate, 0.1% SDS, 10 mmol/l EDTA, and protease inhibitors). After 40 minutes of incubation in ice, samples were sonicated and cleared by centrifugation at 15,000 g at 4°C for 40 min. Supernatants were removed and protein content was determined using the Bradford assay.

CML levels by LC-MS

CML levels were evaluated on plasma and total gastrocnemius extracts after hydrolisis with 0.6 M trichloroacetic acid and 50 μL of hydrochloric acid 6 M for 2 hours at 60°C.

The chromatographic separations were run on an Ultimate 3000 HPLC (Dionex, Milan, Italy) coupled to a high resolving power mass spectrometer (HRMS) LTQ Orbitrap (Thermo Scientific, Rodano, Italy), equipped with an atmospheric pressure interface and an ESI ion source. Samples were analyzed using a Reverse Phase C18 column (Phenomenex Synergi 150 × 2.1 mm, 3 μm particle size) at a flow rate of 200 μL/min. A gradient mobile phase composition was adopted: 95/5 to 40/60 in 25 min, 5 mM heptafluorobutanoic acid/acetonitrile. The monitored protonated molecular ions were 205.1188 *m/z*. Quantitative determination were done by using CML calibration data [6,30].

Western blotting

Equal amounts of proteins were separated by SDS-PAGE and electrotransferred to nitrocellulose membrane. Membranes were probed with primary antibodies followed by incubation with

appropriated HRP-conjugated secondary antibodies. Proteins were detected with ECL detection system and quantified by densitometry using analytic software (Quantity-One, Bio-Rad, Hercules, CA, USA). Results were normalized with respect to α-tubulin densitometric value.

Co-immunoprecipitation.

Equal amounts of total proteins (500 μg) were incubated overnight with 2 μg of rabbit anti-SCAP antibody. The antibody-antigen complexes were then incubated with Protein A Sepharose beads for 3 h. SDS Laemmli buffer was added to the beads and cleared proteins were subjected to SDS–PAGE and immunoblotted with mouse anti-CML antibody and, after stripping, with SCAP antibody.

Immunofluorescence and immunohistochemistry analysis.

CML was analysed by immunohistochemistry on 10 μm gastrocnemius cryostatic sections. After blocking, sections were incubated overnight with primary antibody and subsequently for 1 h with HRP-conjugated secondary antibody and nuclei were counterstained with hematoxylin.

A set of serial sections from the same gastrocnemius area was used for localization of AGE-R1 and SIRT-1 by double indirect immunofluorescence and subsequent identification of the fiber typology by immunohistochemistry. After blocking, sections were incubated overnight with a mix of the primary antibodies and subsequently for 1 h with a mix of Cy3-labelled and FITC-labelled secondary antibodies. Nuclei were stained with Hoechst dye. Sections were then examined using a Leica Olympus epifluorescence microscope (Olympus Bx4I). After immunofluorescence, a serial section from the same sample was analyzed for myosin heavy chain (MHC) 2A isoform expression by immunohistochemistry. The myofibers positive either for AGE-R1/SIRT-1 and MHC 2A were identified by accurate microscopic observations.

SDH enzymatic activity

Fifty μL of protein extracts were incubated with 200 μL reaction buffer containing 10 mM Na-succinate, DCPIP 50 μg/mL, 10 mM phosphate buffer (pH 7.4), 2 mM KCN, 10 mM CaCl2, 0.05% BSA. The absorbance at 600 nm was measured at t0, 3 min and 20 min after the addition of

proteins. The rate of disappearance of the absorbance between 3 and 20 min was corrected for the total protein loaded and used to calculate the SDH enzymatic activity [31].

Staining and image analysis of SDH activity.

Succinic dehydrogenase activity was assessed by incubating 10 μm gastrocnemius sections in 20 mM sodium succinate, 10% nitrotetrazolium blue in 0.2 M phosphate buffer, pH 7.6, substrate solution at 37°C for 40 min. Slides were then washed in distilled water, mounted and imaged. SDH staining intensity for the entire gastrocnemius section was determined using Image J software (NIH) as described by Rinnankoski-Tuikka et al. [32] with slight modifications. Briefly, 4x magnification images (n = 6-12 mice per group) with a minimum of three fields-of-view per muscle cross-section were converted to 8-bit gray-scale (range of grey levels 0–255) images. An intensity threshold representing minimal intensity values corresponding to SDH activity was set manually and uniformly used for all images (least oxidative gray levels 46–90; intermediate oxidative 91-139; most oxidative 140–255). The three intensity scaled fractions representing different oxidative capacities of fibers were expressed as the percentage of total number of SDH-positive myofibers.

Mitochondrial membrane potential.

Gastrocnemius frozen sections were incubated with 500 nmol/L MitoTracker Red CMXRos (Molecular Probes, Eugene, Ore) at 37°C for 45 minutes, that gives a red fluorescence proportional to mitochondrial membrane potential. After washing in PBS, the sections were fixed with 3.7% formaldehyde for 5 minutes [33]. Sections were permeabilized with ice cold acetone for 5 minutes, blocked in 3% BSA in PBS for 30 minutes, and then incubated with MHC 2A antibody followed by FITC-labelled secondary antibody and examined using a Leica Olympus epifluorescence microscope (Olympus Bx4I).

Reactive oxygen species (ROS) staining.

ROS were evaluated by dihydroethidium (DHE) staining on 10 μm cryostatic sections. Sections were incubated with a 1 μM DHE solution for 15 minutes in the dark. After washing sections were mounted and digitised at 10x magnification [34].

Statistical analysis

The Shapiro-Wilk test was used to assess the normality of the variable distributions. One-way ANOVA followed by Bonferroni's post-hoc test were adopted for comparison among the experimental groups. Data were expressed as mean ± standard deviation. Statistical tests were performed with GraphPad Prism 6.0 software package (GraphPad Software, San Diego, CA, USA). Threshold for statistical significance was set to $P<0.05$.

Materials

All compounds were purchased from Sigma Chemical, unless otherwise stated. Primary antibodies are listed in **Supplementary Material**.

Results.

General parameters.

After 12 weeks of diet, HFRT mice still did not show any significant alterations in body weight or body mass composition, while they had slight but significant increase in plasma glucose and insulin levels, higher plasma TG and cholesterol levels (**Table 1**), in comparison to SD mice. The daily calories and drink intake did not differ between SD and HFRT mice, and for the entire protocol duration HFRT mice did not develop polyuria or polydipsia that could interfere with pyridoxamine intake (data not shown). Notably, pyridoxamine supplementation to HFRT mice maintained glucose and lipid plasma profiles quite similar to those of SD.

High-fructose diet generates high levels of AGEs.

Analysis by LC-MS revealed very high levels of CML both in plasma and in gastrocnemius muscle homogenates of HFRT mice (**Fig. 1A**). Immunohistochemistry analysis for CML confirmed a very marked increase of glycation in gastrocnemius sections of HFRT mice with a discrete CML accumulation in specific myofibers (**Fig. 1B**). In addition, Western blotting analysis showed a 4-fold increase in RAGE expression in HFRT compared to SD mice (**Fig. 1C**). On the other hand, in HFRT mice gastrocnemius we observed a dramatic fall in the AGEs detoxifying AGE-receptor 1

(AGE-R1) (**Fig. 1D**). As expected, pyridoxamine supplementation completely prevented AGEs generation. Since RAGE and AGE-R1 expressions are respectively directly and inversely depending on AGEs levels [16,17], as consequence of the prevention of AGEs generation pyridoxamine also inhibited RAGE hyperexpression and effectively prevented AGER1 depletion.

Inhibition of AGEs reduces fructose-induced lipogenesis.

In the skeletal muscle of HFRT mice we detected marked IMCL deposition (**Fig. 2A**), confirmed by higher triglyceride levels in gastrocnemius homogenates (**Fig. 2B**), compared to SD mice.

As shown by Western blotting analysis (**Fig. 2C**), in gastrocnemius muscle from HFRT mice the lipogenic SCAP/SREBP pathway was strongly activated, and the SREBP-1c target genes ACC and FASN were hyperexpressed. In particular, ACC, which is considered the rate limiting enzyme of the fatty acid synthesis, resulted activated as shown by its decreased phospohrylation. Pyridoxamine supplementation inhibited lipogenesis activation and thus almost completely prevented lipid accumulation.

Fructose-derived AGEs exert a multiple interference on SCAP/SREBP pathway.

To investigate the mechanisms by which AGEs can affect the SCAP/SREBP pathway, we performed a co-immunoprecipitation assay, showing that a greater amount of SCAP is glycated by CML in gastrocnemius of HFRT mice compared to SD, while SCAP glycation is almost completely prevented by pyridoxamine supplementation (**Fig. 3A**).

Moreover, we assessed the expression of SIRT-1, a deacetylase that regulates many transcriptional proteins important in energy metabolism, recently emerged as inhibitor of SREBP-1c activity and thought to be regulated by AGE-R1 [17]. Actually, besides the reduced levels of AGE-R1 induced by the HFRT diet, we also observed a reduction in SIRT-1 expression, which was effectively prevented by pyridoxamine treatment (**Fig. 3B**). Interestingly, double immunofluorescence analysis in gastrocnemius from SD mice showed that AGER1 and SIRT1 are localized in the same myofibers (**Fig. 3C**). Specifically, AGE-R1 was located along the plasmamembranes, while SIRT-1 had a cytoplasmic distribution. Interestingly, the immunohistochemistry for the MHC 2A isoform

performed on sections sequential to that used for the AGE-R1/SIRT-1 immunofluorescence, shown that they where exclusively expressed in myofibers having an oxidative metabolism (**Fig. 3D**).

Inhibition of AGEs restores myogenic regulatory factors (MRFs) expression, fiber type and metabolism of muscle altered by fructose feeding.

Since MRFs, which are involved in muscle structural proteins reprogramming, are suggested to be controlled by SREBP-1c activity [35], we analysed their expression in gastrocnemius. Our results showed that MyoD1 and MEF2c were downregulated, while myogenin was strongly upregulated by HFRT diet. Unexpectedly, pyridoxamine supplementation maintained the expression pattern of MRFs similar to that recorded in SD condition (**Fig. 4A**).

Since the structural proteins reprogramming regulated by the MRFs may induce alterations in the fiber type composition, we assessed the expression levels of the three main isoforms of MHC. In gastrocnemius of HFRT mice, we observed a higher content of the MHC isoforms 1 and 2A, which are specifically expressed by the myofibers with an oxidative metabolism, and a lower content in fast glycolytic MHC 2B (**Fig. 4B**). This specific composition was associated to an increased expression of either the cytoplamsic subunit of the succinic dehydrogenase (SDHA), a marker of mitochondria biogenesis, and the muscle carnitine palmytoiltransferase-1 (CPT-1m), the limiting enzyme of the mitochondrial β-oxidation (**Fig. 4C**). Notably, the pyridoxamine supplementation preserved the myosin heavy chain composition and the metabolic features of the normal gastrocnemius.

Inhibition of AGEs preserves mitochondrial efficiency affected by fructose.

To assess whether the increased number of oxidative myofibers and mitochondria were paralleled by increased mitochondrial function, we evaluated enzymatic activity of the SDH in gastrocnemius cross sections (**Fig. 5A**). In the whole gastrocnemius muscle of HFRT mice an increase in SDH enzymatic activity (**Fig. 5B**) and in SDH-positive myofibers was detected (**Fig. 5C**). However, despite increased total number of oxidative myofibers, the percentage of most oxidative myofibers was significantly reduced, while only least oxidative myofibers were increased (**Fig. 5D**). Thus, the

average activity of SDH per single oxidative myofiber in HFRT mice resulted reduced compared to the SD mice. Pyridoxamine supplementation to HFRT fed mice, although limiting the increase in total number of SDH-positive myofibers, markedly raised the number of intermediate oxidative myofibers, thus improving individual myofibers oxidative efficiency. The hypothesis of a mitochondrial impairment induced by the fructose-derived AGEs was further confirmed by the Mitotracker assay performed on cryostatic muscle sections, showing a reduced mitochondrial membrane potential, normalized for the number of MHC 2A-positive myofibers, in the HFRT gastrocnemius (**Fig. 5E**), and by the reduced amount of sMtCK in HFRT gastrocnemius extracts (**Fig. 5F**). The pyridoxamine treatment maintained the mitochondrial membrane potential and the energy supply near to the SD values.

This reduced mitochondrial efficiency was paralleled by increased generation of ROS revealed by DHE staining (**Fig. 6A**) and induction of the mitochondrial superoxide dismutase (MnSOD) (**Fig. 6B**). Pyridoxamine was able to prevent oxidative stress and MnSOD expression increase, in keeping with its known antioxidant activity.

Inhibition of AGEs preserves muscle efficiency.

According to either a reduced glycolytic and an inefficient oxidative metabolism, functional assessment on gastrocnemius muscle revealed reduced forelimb strenght (-16% of SD value) paralleled by a more markedly increased fatigability (-32% of SD resistance) (**Table 2**). Notably, since body weight did not differ between SD and HFRT mice, the reduced performance of HFRT mice in the Kondziela's inverted screen test can not be due to overweight. Interestingly, pyridoxamine supplementation improved both grip strength and resistance to fatigue affected by the HFRT diet.

Discussion

The present study provides new knowledge on the effects of fructose-derived AGEs in skeletal muscle morphology and metabolism, which are shown to be mediated by the deregulation of

SREBP-1c. We have recently observed that AGEs overproduction in mice liver and skeletal muscle is associated to increased lipogenesis due to the activation of SREBP-1c [6,26]. We also demonstrated in obese mice gastrocnemius a marked fiber type transition towards a more oxidative metabolism associated to specific IMCL and AGEs accumulation in the oxidative myofibers [26]. However, a causal link between AGEs and SREBP-1c activation, as well as an evaluation of muscle function and mitochondria efficiency, were lacking. Besides, it was not possible to gather the dietary source of endogenous AGEs since either a high intake of fat and sugar or an energy overload were able to induce AGEs accumulation in gastrocnemius muscle. Conversely, in the present study we used only fructose as main source of AGEs. The choice of focusing on fructose-derived AGEs is based on recent epidemiological data showing a dramatic rise in free fructose consumption due to the wide employment of high fructose corn syrup in the preparation of foods and beverages [3]. Indeed, we here demonstrated that a high fructose intake evoked endogenous CML production and lipogenesis activation and the use of pyridoxamine, besides the effective inhibition of CML production, was able to improve plasma glycolipidic profile and to reduce gastrocnemius muscle lipogenesis.

Previous in vitro studies demonstrated that the glycation of SCAP, which escorts SREBP-1c from the endoplasmic reticulum to the Golgi where it is activated by a cleavage, prevents its physiological proteasomal degradation and prolongs its half-life, thus promoting its recycling between the endoplasmic reticulum and the Golgi and prolonging its action on SREBP-1c activity [36,37]. Furthermore, the increased levels of SCAP here reported in the gastrocnemius of HFRT mice can be the result of both its reduced degradation rate and the SREBP1c transcriptional activity, which also has SCAP among its target genes. In this perspective the reduction of SCAP glycation by pyridoxamine, promotes its degradation, thus limiting SREBP activation and reducing SCAP levels, definitively confirming a direct role of AGEs in the deregulation of SCAP/SREBP pathway.

On the other hand, SREBP-1c activity can be downregulated through deacetylation by SIRT-1 [38], a NAD(+)-dependent protein deacetylase that regulates fat mobilization and fatty acid oxidation and

increases insulin sensitivity and gluoconeogenesis [39]. The induction of SIRT-1 activity has been demonstrated to prevent insulin resistance and fat accumulation by enhancing mitochondrial biogenesis and β-oxidation [39]. In contrast, in high-fat diet or metabolic challenges, hepatic SIRT-1 depletion increases acetylation of SREBP-1c with enhanced lipogenic gene expression [38,40]. Besides, the in vivo activity of SIRT-1 has been proved to depend on the protective functions of AGE-R1. Specifically, in differentiated 3T3-L1 adipocytes, transduced or silenced for AGE-R1and stimulated with the CML precursor methylglyoxal, SIRT-1 expression was found to be inversely correlated to methylglyoxal doses [41]. Furthermore, AGEs oral administration has been reported to induce downregulation of both AGE-R1 and SIRT-1, while AGEs restriction normalized their expression levels with a concomitant attenuation of RAGE and reduced lipid synthesis. That work also demonstrated by genetically modulation of AGE-R1 expression in monocytes that SIRT-1 expression and function are strictly correlated to AGE-R1 efficiency [17]. Consistent with these findings, we observed that the parallel reduction of AGE-R1 and SIRT-1 expression in muscle of HFRT mice was efficiently prevented by the inhibition of AGEs formation by pyridoxamine. Thus, it can be argued that AGEs interfere with SREBP-1c activation by either the direct glycation of SCAP and the downregulation of AGE-R1/SIRT-1 pathway, leading in both cases to enhanced lipogenesis. To our knowledge, this is the first evidence of a multiple interference of AGEs on lipid metabolism in skeletal muscle.

The skeletal muscle comprises different fiber types, whose identity is established during differentiation by MRFs [42-44]. These factors regulate the differential expression of MHC isoforms defining three major fiber types that rely on different metabolic pathways for energy production: slow-twitch oxidative fibers, containing MHC 1, fast-twitch oxidative fibers, containing MHC 2A, and fast-twitch glycolytic fibers, containing MHC 2B [45]. Thus, muscle fibers can change their properties through a fiber type-specific regulation of MHC gene expression in response to modifications in diet composition [26,46,47]. AGE-R1 and SIRT-1 colocalization in MHC 2A-expressing myofibers is consistent with our previous findings showing a preferential accumulation

of both CML and IMCL in oxidative fibers [26], suggesting a crosstalk between AGEs-induced lipogenesis and structural muscle proteins expression. For instance, a further very interesting and unexplored fallout of the AGEs-mediated activation of SREBP-1c is related to a new transcriptional role for SREBP-1c highlighted by recent works [35, 48]. They reported that SREBP-1c controls the transcription of MRFs which are responsible for the regulation of myogenesis and the setting of muscle fiber type composition [42,43]. In *in vitro* studies, SREBP-1c overexpression inhibits myotube differentiation and induces myofibers atrophy [48]. Indeed, it has been observed that the expression of MRFs and muscle structural proteins, as MHC, is strictly regulated by the modulation of SREBP-1c activity in mice [35]. In our model, fructose feeding evoked a dramatic alteration in MRFs content, with reduced MyoD and MEF2C levels and increased myogenin levels. These alterations could be related to the observed modification in MHC isoforms expression, accounting for a glycolytic-to-oxidative fiber type transition. In keeping with our results, there are indications from the literature that MyoD1 and MEF2C actually regulate the expression of the glycolytic MHC 2B [42], while myogenin is associated to the expression of the oxidative isoforms MHC 1 and 2A [43]. Moreover, it has been reported that RAGE, which is transiently hyperexpressed in injured muscle, positively regulates myoblast differentiation by directly increasing myogenin expression [49]. Intriguingly, in our model the preservation of MRFs expression levels and the fiber type composition by the inhibition of AGEs generation obtained by pyridoxamine treatment in HFRT mice strongly suggests, for the first time, that AGEs could be involved in muscle proteins reprogramming through either SREBP-1c activation and RAGE induction. Our results are in keeping with several studies showing the diet-induced myofibers type transition towards oxidative isoforms as a physiological adaptation to the rise in fatty acid availability [46,47,50]. However, although in some animal models of diet-induced obesity an increase in mitochondrial oxidative capacity has been observed [51,52], it is elsewhere reported that the increase in oxidative fibers in response to fatty acids overload could not be necessarily accompanied by an increased mitochondrial efficiency [47]. Furthermore, studies in humans, reviewed by Sivitz and Yorek [53],

have shown that type 2 diabetic patients exhibited alteration in mitochondrial morphology, and a decrease in the activity of the respiratory chain and expression of the enzymes of oxidative mitochondrial metabolism. It has been proposed that in diet-induced obesity, after the early induction of mitochondria biogenesis and β-oxidation, the fatty acid overload to mitochondria generates high levels of lipid peroxidation as well as an oxidative stress condition [54,55]. In our model, the HFRT-induced increased number of oxidative myofibers, as well as the increased expression of β-oxidation and mitogenesis markers, may suggest an adaptive upregulation of oxidative metabolism aimed to metabolize fatty acid overproduction. However, our results on SDH activity in individual oxidative myofibers of HFRT mice indicate a reduced oxidative phosphorylation chain efficiency. This impaired oxidative activity leads to lowered mitochondrial membrane potential, as revealed by reduced Mitotracker staining in the HFRT gastrocnemius, which is an indicator of decreased ATP production [56]. The diminished mitochondrial energy production in the whole gastrocnemius of HFRT mice is confirmed by the reduced expression of sMtCK, the enzyme mainly expressed in oxidative myofibers coupled to oxidative phosphorylation and responsible for the transfer of phosphate from mitochondrial ATP to cytosolic creatine [57]. Reduced levels of sMtCK have been previously observed in certain myopathies and are linked to compromised energy availability [58].The effective preservation of mitochondrial efficiency by pyridoxamine strongly support the causal role of fructose-derived AGEs. According to the hypothesis of an impairment of mitochondrial functions induced by fructose-derived AGEs, namely β-oxidation and SDH activity, that failed to remove fatty acid surplus, we also found increased oxidative stress parameters that could also contribute to exacerbate AGEs production. The recognized anti-oxidative activity of pyridoxamine, together with its effect on the restoration of AGE-R1 and SIRT-1 levels, which are also known to be provided with antioxidant effects [17,41], may also contrast the mitochondrial generation of oxidative stress. These aspects should be further explored in a future work to clarify the fallout of diet-derived AGEs on mitochondria integrity, since accumulating data report the induction of mitochondria disruption and autophagy by AGEs in

several experimental conditions [59,60]. Finally, this picture of general mitochondrial exhaustion induced by HFRT diet could account for the significantly reduced force and fatigability observed in HFRT mice when subjected to Kondziela's and grip tests. Pyridoxamine supplementation to HFRT mice completely prevented this functional deficit, probably as a result of the effects of inhibition of AGEs formation on lipogenesis and muscle metabolism.

Taken together, the present data extend our previous knowledge and indicate for the first time that fructose-derived AGEs exert a multiple interference on SREBP-1c activity which in turn enhances fatty acids synthesis and impairs muscle proteins expression, leading to an ineffective crosstalk between lipogenesis and muscle reprogramming that could chronically contribute to progression towards muscle impairment (**Fig. 7**). In consideration of the worldwide rapid rise in metabolic diseases due to the increasing consumption of sugar-rich foods and drinks, it is of relevance to thoroughly understand the impact of endogenous AGEs in human health. In this perspective, further research are needed to identify new effective strategies to counteract AGEs generation or potentiate AGEs-detoxifying systems to prevent metabolic diseases and related complications. In particular, the marked protective effect of pyridoxamine here reported on muscle metabolism and function does encourage a wider exploration of its therapeutic potential in human diseases.

Acknowledgments

This study was supported by a grant of CRT Foundation (2010.1954): "Consuming of sugar-added drinks as risk factor for metabolic diseases: emerging role of fructose" and by grants from University of Turin, Ricerca Locale ex-60. No potential conflicts of interest relevant to this article were reported.

References

[1] McGuinness, O.P.; Cherrington, A.D. Effects of fructose on hepatic glucose metabolism. Curr. Opin. Clin. Nutr. Metab. Care 6:441-448; 2003.

[2] Bray, G.A.; Nielsen, S.J.; Popkin, B.M. Consumption of high-fructose corn syrup in beverages may play a role in the epidemic of obesity. Am. J. Clin. Nutr. 79(4):537-543; 2004.

[3] Tappy, L. Lê, K.A. Metabolic effects of fructose and the worldwide increase in obesity. Physiol. Rev. 90(1):23-46; 2010.

[4] Stanhope, K.L.; Schwarz, J.M.; Havel, P.J. Adverse metabolic effects of dietary fructose: results from the recent epidemiological, clinical, and mechanistic studies. Curr. Opin. Lipidol. 24(3):198-206; 2013.

[5] Lakhan, S.E.; Kirchgessner, A. The emerging role of dietary fructose in obesity and cognitive decline. Nutr. J. 12:114; 2013.

[6] Mastrocola, R.; Collino, M.; Rogazzo, M.; Medana, C.; Nigro, D.; Boccuzzi, G.; Aragno, M. Advanced glycation end products promote hepatosteatosis by interfering with SCAP-SREBP pathway in fructose-drinking mice. Am. J. Physiol. Gastrointest. Liver Physiol. 305(6):G398-407; 2013.

[7] Vistoli, G.; De Maddis, D.; Cipak, A.; Zarkovic, N.; Carini, M.; Aldini, G. Advanced glycoxidation and lipoxidation end products (AGEs and ALEs): an overview of their mechanisms of formation. Free Rad. Res. 47(S1):3-27; 2013.

[8] Vlassara, H.; Striker, G.E. Advanced glycation endproducts in diabetes and diabetic complications. Endocrinol. Metab. Clin. North Am. 42(4):697-719; 2013.

[9] Van Puyvelde, K.; Mets, T.; Njemini, R.; Beyer, I.; Bautmans, I. Effect of advanced glycation end product intake on inflammation and aging: a systematic review. Nutr. Rev. 72(10):638-50; 2014.

[10] Levi, B.; Werman, M.J. Long-term fructose consumption accelerates glycation and several age-related variables in male rats. J. Nutr. 128(9):1442-1449; 1998.

[11] Lingelbach, L.B.; Mitchell, A.E.; Rucker, R.B.; McDonald, R.B. Accumulation of advanced glycation endproducts in aging male Fischer 344 rats during long-term feeding of various dietary carbohydrates. J. Nutr. 130(5):1247-1255; 2000.

[12] Davis, K.E.; Prasad, C.; Vijayagopal, P.; Juma, S.; Imrhan, V. Serum soluble receptor for advanced glycation end products correlates inversely with measures of adiposity in young adults. Nutr. Res. 34(6):478-485; 2014.

[13] Jia, X.; Chang, T.; Wilson, T.W.; Wu, L. Methylglyoxal mediates adipocyte proliferation by increasing phosphorylation of Akt1. PLoS One 7(5):e36610; 2012.

[14] Cai, W.; Uribarri, J.;, Zhu, L.; Chen, X.; Swamy, S.; Zhao, Z.; Grosjean, F.; Simonaro, C.; Kuchel, G.A.; Schnaider-Beeri, M.; Woodward, M.; Striker, G.E.; Vlassara, H. Oral glycotoxins are a modifiable cause of dementia and the metabolic syndrome in mice and humans. PNAS 111(13):4940-4945; 2014.

[15] Gaens, K.H.; Niessen, P.M.; Rensen, S.S.; Buurman, W.A.; Greve, J.W.; Driessen, A.; Wolfs, M.G.; Hofker, M.H.; Bloemen, J.G.; Dejong, C.H.; Stehouwer, C.D.; Schalkwijk, C.G. Endogenous formation of Nε-(carboxymethyl)lysine is increased in fatty livers and induces inflammatory markers in an in vitro model of hepatic steatosis. J. Hepatol. 56(3):647-655; 2012.

[16] de la Maza, M.P.; Uribarri, J.; Olivares, D.; Hirsch, S.; Leiva, L.; Barrera, G.; Bunout, D. Weight increase is associated with skeletal muscle immunostaining for advanced glycation end products, receptor for advanced glycation end products, and oxidation injury. Rejuvenation Res. 11(6):1041-1048; 2008.

[17] Uribarri, J.; Cai, W.; Ramdas, M.; Goodman, S.; Pyzik, R.; Chen, X.; Zhu, L.; Striker, G.E.; Vlassara, H. Restriction of advanced glycation end products improves insulin resistance in human type 2 diabetes: potential role of AGER1 and SIRT1. Diabetes Care 34(7):1610-1616; 2011.

[18] Hagiwara, S.; Gohda, T.; Tanimoto, M.; Ito, T.; Murakoshi, M.; Ohara, I.; Yamazaki, T.; Matsumoto, M.; Horikoshi, S.; Funabiki, K.; Tomino, Y. Effects of pyridoxamine (K-163) on glucose intolerance and obesity in high-fat diet C57BL/6J mice. Metabolism 58(7):934-945; 2009.

[19] Voziyan, P.A.; Hudson, B.G. Pyridoxamine as a multifunctional pharmaceutical: targeting pathogenic glycation and oxidative damage. Cell. Mol. Life Sci. 62(15):1671-1681; 2005.

[20] Degenhardt ,T.P.; Alderson, N.L.; Arrington, D.D.; Beattie, R.J.; Basgen, J.M.; Steffes, M.W.; Thorpe, S.R.; Baynes, J.W. Pyridoxamine inhibits early renal disease and dyslipidemia in the streptozotocin-diabetic rat. Kidney Int 61(3):939-950; 2002.

[21] Price, D.L.; Rhett, P.M.; Thorpe, S.R.; Baynes, J.W. Chelating activity of advanced glycation end-product inhibitors. J. Biol. Chem. 276(52):48967-48972; 2001.

[22] Engelen, L.; Stehouwer, C.D.; Schalkwijk, C.G. Current therapeutic interventions in the glycation pathway: evidence from clinical studies. Diabetes Obesity Metab. 15(8):677-689; 2013.

[23] Aldini, G.; Vistoli, G.; Stefek, M.; Chondrogianni, N.; Grune, T.; Sereikaite, J.; Sadowska-Bartosz, I.; Bartosz, G. Molecular strategies to prevent, inhibit, and degrade advanced glycoxidation and advanced lipoxidation end products. Free Rad. Res. 47 Suppl 1:93-137; 2013.

[24] Cai, W.; He, J.C.; Zhu, L.; Lu, C.; Vlassara, H. Advanced glycation end product (AGE) receptor 1 suppresses cell oxidant stress and activation signaling via EGF receptor. Proc. Natl. Acad. Sci. USA 103(37):13801-13806; 2006.

[25] Ramamurthy, B.; Larsson, L. Detection of an aging-related increase in advanced glycation end products in fast- and slow-twitch skeletal muscles in the rat. Biogerontology 14(3):293-301; 2013.

[26] Mastrocola, R.; Collino, M.; Nigro, D.; Chiazza, F.; D'Antona, G.; Aragno, M.; Minetto, M.A. Accumulation of advanced glycation end-products and activation of the SCAP/SREBP

Lipogenetic pathway occur in diet-induced obese mouse skeletal muscle. PlosOne 10(3):e0119587; 2015.

[27] Watson, A.M.; Soro-Paavonen, A.; Sheehy, K.; Li, J.; Calkin, A.C.; Koitka, A.; Rajan, S.N.; Brasacchio, D.; Allen, T.J.; Cooper, M.E.; Thomas, M.C.; Jandeleit-Dahm, K.J. Delayed intervention with AGE inhibitors attenuates the progression of diabetes-accelerated atherosclerosis in diabetic apolipoprotein E knockout mice. Diabetologia 54(3):681-9; 2011. doi: 10.1007/s00125-010-2000-9.

[28] Deacon, R.M. Measuring the strength of mice. J Vis Exp (76); 2013.

[29] MacArthur, D.G.; Seto, J.T.; Chan, S.; Quinlan, K.G.; Raftery, J.M.; Turner, N.; Kee, A..J.; Hardeman, E.C.; Gunning, P.W.; Cooney, G.J.; Head, S.I.; Yang, N.; North, K.N. An Actn3 knockout mouse provides mechanistic insights into the association between alpha-actinin-3 deficiency and human athletic performance. Hum. Mol. Gen. 17(8):1076-1086; 2008.

[30] Kuang, L.; Jing, Z.; Wang, J.; Ma, L.; Liu, X.; Yang, J. Quantitative determination of ε-N-carboxymethyl-l-lysine in human plasma by liquid chromatography-tandem mass spectrometry. J. Pharm. Biomed. Anal. 90:1-6; 2014. doi: 10.1016/j.jpba.2013.11.003.

[31] Fontes-Oliveira CC, Busquets S, Toledo M, Penna F, Paz Aylwin M, Sirisi S, Silva AP, Orpí M, García A, Sette A, Inês Genovese M, Olivan M, López-Soriano FJ, Argilés JM (2013) Mitochondrial and sarcoplasmic reticulum abnormalities in cancer cachexia: altered energetic efficiency? Biochim Biophys Acta 1830(3):2770-8

[32] Rinnankoski-Tuikka, R.; Silvennoinen, M.; Torvinen, S.; Hulmi, J.J.; Lehti, M.; Kivelä, R.; Reunanen, H.; Kainulainen, H. Effects of high-fat diet and physical activity on pyruvate dehydrogenase kinase-4 in mouse skeletal muscle. Nutr. Metab. 9(1):53; 2012.

[33] Matsushima, S.; Ide, T.; Yamato, M.; Matsusaka, H.; Hattori, F.; Ikeuchi, M.; Kubota, T.; Sunagawa, K.; Hasegawa, Y.; Kurihara, T.; Oikawa, S.; Kinugawa, S.; Tsutsui, H. Overexpression of mitochondrial peroxiredoxin-3 prevents left ventricular remodeling and failure after myocardial infarction in mice. Circulation 113(14):1779-86; 2006.

[34] Dikalov, S.; Griendling, K.K.; Harrison, D.G. Measurement of reactive oxygen species in cardiovascular studies Hypertension 49:717-727; 2007.

[35] Dessalle, K.; Euthine, V.; Chanon, S.; Delarichaudy, J.; Fujii, I.; Rome, S.; Vidal, H.; Nemoz, G.; Simon, C.; Lefai, E. SREBP-1 transcription factors regulate skeletal muscle cell size by controlling protein synthesis through myogenic regulatory factors. PlosOne 7(11):e50878; 2012.

[36] Yuan, Y.; Zhao, L.; Chen, Y.; Moorhead, J.F.; Varghese, Z.; Powis, S.H.; Minogue, S.; Sun, Z.; Ruan, X.Z. Advanced glycation end products (AGEs) increase human mesangial foam cell formation by increasing Golgi SCAP glycosylation in vitro. Am. J. Physiol. Renal Physiol. 301(1):F236-43; 2011. doi: 10.1152/ajprenal.00646.2010.

[37] Zhou, C.; Lei, H.; Chen, Y.; Liu, Q.; Li, L.C.; Moorhead, J.F.; Varghese, Z.; Ruan, X.Z. Enhanced SCAP glycosylation by inflammation induces macrophage foam cell formation. PLoS One 8(10):e75650; 2013. doi: 10.1371/journal.pone.0075650

[38] Ponugoti, B.; Kim, D.H.; Xiao, Z.; Smith, Z.; Miao, J.; Zang, M.; Wu, S.Y.; Chiang, C.M.; Veenstra, T.D.; Kemper, J.K. SIRT1 deacetylates and inhibits SREBP-1C activity in regulation of hepatic lipid metabolism. J. Biol. Chem. 285(44):33959-33970; 2010.

[39] Guarente, L.; Franklin, H. Epstein Lecture: Sirtuins, aging, and medicine. N. Engl. J. Med. 364(23):2235-2244; 2011.

[40] Walker, A.K.; Yang, F.; Jiang, K.; Ji, J.Y.; Watts, J.L.; Purushotham, A.; Boss, O.; Hirsch, M.L.; Ribich, S.; Smith, J.J.; Israelian, K.; Westphal, C.H.; Rodgers, J.T.; Shioda, T.; Elson, S.L.; Mulligan, P.; Najafi-Shoushtari, H.; Black, J.C.; Thakur, J.K.; Kadyk, L.C.; Whetstine, J.R.; Mostoslavsky, R.; Puigserver, P.; Li, X.; Dyson, N.J.; Hart, A.C.; Näär, A.M. Conserved role of SIRT1 orthologs in fasting-dependent inhibition of the lipid/cholesterol regulator SREBP. Genes Develop. 24(13):1403-1417; 2010.

[41] Cai, W.; Ramdas, M.; Zhu, L.; Chen, X.; Striker, G.E.; Vlassara, H. Oral advanced glycation endproducts (AGEs) promote insulin resistance and diabetes by depleting the antioxidant defenses AGE receptor-1 and sirtuin 1. PNAS 109(39):15888-15893; 2012.

[42] Hennebry, A.; Berry, C.; Siriett, V.; O'Callaghan, P.; Chau, L.; Watson, T.; Sharma, M.; Kambadur, R. Myostatin regulates fiber-type composition of skeletal muscle by regulating MEF2 and MyoD gene expression. Am. J. Physiol. Cell. Physiol. 296(3):C525-534; 2009.

[43] Zhu, L.N.; Ren, Y.; Chen, J.Q.; Wang, Y.Z. Effects of myogenin on muscle fiber types and key metabolic enzymes in gene transfer mice and C2C12 myoblasts. Gene 532(2):246-552; 2013.

[44] Meissner, J.D.; Chang, K.C.; Kubis, H.P.; Nebreda, A.R.; Gros, G.; Scheibe, R.J. The p38alpha/beta mitogen-activated protein kinases mediate recruitment of CREB-binding protein to preserve fast myosin heavy chain IId/x gene activity in myotubes. J. Biol. Chem. 282(10):7265-7275; 2007.

[45] Graziotti, G.H.; Ríos, C.M.; Rivero, J.L. Evidence for three fast myosin heavy chain isoforms in type II skeletal muscle fibers in the adult llama (Lama glama). J. Histochem. Cytochem. 49(8):1033-44; 2001.

[46] Shortreed, K.E.; Krause, M.P.; Huang, J.H.; Dhanani, D.; Moradi, J.; Ceddia, R.B.; Hawke, T.J. Muscle-specific adaptations, impaired oxidative capacity and maintenance of contractile function characterize diet-induced obese mouse skeletal muscle. PlosOne 4(10):e7293; 2009.

[47] de Wilde, J.; Mohren, R.; van den Berg, S.; Boekschoten, M,; Dijk, K.W.; de Groot, P.; Müller, M.; Mariman, E.; Smit, E. Short-term high fat-feeding results in morphological and metabolic adaptations in the skeletal muscle of C57BL/6J mice. Physiol. Genomics. 32(3):360-369; 2008.

[48] Lecomte, V.; Meugnier, E.; Euthine, V.; Durand, C.; Freyssenet, D.; Nemoz, G.; Rome, S.; Vidal, H.; Lefai, E. A new role for sterol regulatory element binding protein 1 transcription factors in the regulation of muscle mass and muscle cell differentiation. Mol. Cell. Biol. 30(5):1182-1198; 2010.

[49] Riuzzi, F.; Sorci, G.; Sagheddu, R.; Donato, R. HMGB1-RAGE regulates muscle satellite cell homeostasis through p38-MAPK- and myogenin-dependent repression of Pax7 transcription. J. Cell Sci. 125(Pt 6):1440-1454; 2012.

[50] Mizunoya, W.; Iwamoto, Y.; Shirouchi, B.; Sato, M.; Komiya, Y.; Razin, F.R.; Tatsumi, R.; Sato, Y.; Nakamura, M.; Ikeuchi, Y. Dietary fat influences the expression of contractile and metabolic genes in rat skeletal muscle. PlosOne 8(11):e80152; 2013.

[51] Koves, T.R.; Ussher, J.R.; Noland, R.C.; Slentz, D.; Mosedale, M.; Ilkayeva, O.; Bain, J.; Stevens, R.; Dyck, J.R.; Newgard, C.B.; Lopaschuk, G.D.; Muoio, D.M. Mitochondrial overload and incomplete fatty acid oxidation contribute to skeletal muscle insulin resistance. Cell. Metab. 7(1):45-56; 2008.

[52] Crescenzo, R.; Bianco, F.; Coppola, P.; Mazzoli, A.; Cigliano, L.; Liverini, G.; Iossa, S. Increased skeletal muscle mitochondrial efficiency in rats with fructose-induced alteration in glucose tolerance. Br. J. Nutr. 110(11):1996-2003; 2013.

[53] Sivitz, W.I.; Yorek, M.A. Mitochondrial dysfunction in diabetes: from molecular mechanisms to functional significance and therapeutic opportunities. Antiox. Redox Signal. 12(4):537-577; 2010.

[54] Chanseaume, E.; Giraudet, C.; Gryson, C.; Walrand, S.; Rousset, P.; Boirie, Y.; Morio, B. Enhanced muscle mixed and mitochondrial protein synthesis rates after a high-fat or high-sucrose diet. Obesity 15(4):853-859; 2007.

[55] Crescenzo, R.; Bianco, F.; Mazzoli, A.; Giacco, A.; Liverini, G.; Iossa, S. Mitochondrial efficiency and insulin resistance. Front. Physiol. 5:512; 2015.

[56] Barbieri, E.; Battistelli, M.; Casadei, L.; Vallorani, L.; Piccoli, G.; Guescini, M.; Gioacchini, A.M.; Polidori, E.; Zeppa, S.; Ceccaroli, P.; Stocchi, L.; Stocchi, V.; Falcieri, E. Morphofunctional and Biochemical Approaches for Studying Mitochondrial Changes during Myoblasts Differentiation. J Aging Res 2011:845379; 2011.

[57] Qin, W.; Khuchua, Z.; Boero, J.; Payne, R.M.; Strauss, A.W. Oxidative myocytes of heart and skeletal muscle express abundant sarcomeric mitochondrial creatine kinase. Histochem. J. 31(6):357-65; 1999.

[58] Tarnopolsky, M.A.; Parshad, A.; Walzel, B.; Schlattner, U.; Wallimann, T. Creatine transporter and mitochondrial creatine kinase protein content in myopathies. Muscle Nerve 24(5):682-8; 2001.

[59] Wang, X.; Yu, S.; Wang, C.Y.; Wang, Y.; Liu, H.X.; Cui, Y.; Zhang, L.D. Advanced glycation end products induce oxidative stress and mitochondrial dysfunction in SH-SY5Y cells. In Vitro Cell. Dev. Biol. Anim. 51(2):204-209; 2015.

[60] Yang, Q.; Guo, S.; Wang, S.; Qian, Y.; Tai, H.; Chen, Z. Advanced glycation end products-induced chondrocyte apoptosis through mitochondrial dysfunction in cultured rabbit chondrocyte. Fundam. Clin. Pharmacol. 29(1):54-61; 2015.

Table 1. General parameters of mice fed a standard diet (SD) or a high-fructose diet (HFRT) for 12 weeks, supplemented or not with 150 mg/kg b.w./day pyridoxamine . Data are means ± standard deviation. Statistical significance: [a]$P<0.05$; [b]$P<0.001$ vs SD.

	SD (n=8)	**SD+P** (n=6)	**HFRT** (n=12)	**HFRT+P** (n=12)
Body weight increase (g)	8.1 ± 1.2	8.4 ± 1.6	9.3 ± 1.6	8.8 ± 1.4
Gastrocnemius weight (% of b. w.)	1.06 ± 0.09	1.06 ± 0.04	1.06 ± 0.07	1.02 ± 0.05
Fasting plasma glucose (mg/dL)	69 ± 19	62 ± 16	91 ± 11[a]	75 ± 16
Fasting plasma insulin (mg/dL)	79.2 ± 4.7	78.1 ± 1.5	86.6 ± 7.1[a]	79.1 ± 6.3
Plasma TG (mg/dL)	30.7 ± 6.6	29.3 ± 5.5	45.5 ± 5.0[b]	37.2 ± 5.6
Plasma Chol (mg/dL)	77.2 ± 6.1	73.9 ± 9.3	115.3 ± 12.5[b]	101.6 ± 18.4[a]

Table 2. Tests for limb resistance to fatigue and muscle strenght of SD or HFRT mice, supplemented or not with 150 mg/kg b.w./die pyridoxamine. Data are means ± standard deviation. Statistical significance: [a]*P*<0.05 vs SD; [c]*P*<0.05 vs HFRT.

	SD (n=8)	**SD+P** (n=6)	**HFRT** (n=12)	**HFRT+P** (n=12)
Kondziela's test (min)	14.5 ± 4.4	14.0 ± 4.3	9.8 ± 2.8[a]	14.4 ± 2.6[c]
Grip test (N)	1.29 ± 0.09	1.28 ± 0.16	1.08 ± 0.09[a]	1.20 ± 0.15

Figure legends

Fig. 1. Fructose-induced AGEs production and AGEs-receptors analysis. (A) Carboxy methyllysine levels evaluated by GC-MS in plasma and gastrocnemius muscle homogenates from SD and HFRT mice, supplemented or not with pyridoxamine. (B) Representative 10x magnification photomicrographs of immunohistochemistry for CML on gastrocnemius sections. (C) Representative Western blots in total gastrocnemius extracts for the pro-inflammatory AGE-receptor RAGE, and (D) the AGEs detoxifying receptor AGE-R1. Histograms report densitometric analyses normalized for the relative tubulin content. Data are means ± standard deviation of 6-12 mice per group. $^{b}P<0.001$ vs SD; $^{d}P<0.001$ vs HFRT.

Fig. 2. Intramyocellular lipid accumulation, triglyceride content, and SCAP/SREBP pathway analysis. (A) Representative 20/40x magnification photomicrographs of Oil Red staining on gastrocnemius. (B) TG content in gastrocnemius homogenates of the four experimental groups. (C) Representative Western blots in total gastrocnemius extracts for SCAP and the active form of SREBP-1c, and (D) for the SREBP-1c target genes FASN and ACC, and the phosphoryaleted form of ACC. Histograms report densitometric analyses normalized for tubulin content. ACC activation is reported as ratio between total ACC and inactive Ser79 phosphorylated form. Data are means ± standard deviation of 6-12 mice per group. $^{a}P<0.05$, $^{b}P<0.001$ vs SD; $^{c}P<0.05$, $^{d}P<0.001$ vs HFRT.

Fig. 3. SCAP glycation rate and SIRT-1 expression and colocalization with AGE-R1. (A) Representative co-immunoprecipitation analysis for the evaluation of SCAP glycation in total gastrocnemius extracts. The upper band reports the reactivity of the immunoprecipitated SCAP with anti-CML antibody, while the lower band reports the reactivity with anti-SCAP antibody as loading control. Histogram reports ratio of densitometric value of CML-glycated SCAP to total SCAP. (B) Representative Western blots in total gastrocnemius extracts for SIRT-1. Histogram reports densitometric analyses of 6-12 mice per group normalized for the relative tubulin content. (C) Representative 40x magnification photomicrographs of immunofluorescence for AGE-R1 and SIRT-1 localization on gastrocnemius sections. (D) Immunohistochemistry analysis for MHC 2A

on serial sections showing specificity of both AGE-R1 and SIRT-1 expression in oxidative myofibers. [b]*P*<0.001 vs SD; [c]*P*<0.05, [d]*P*<0.001 vs HFRT.

Fig. 4. Myogenic regulatory factors (MRFs) expression, myosin heavy chain isoforms composition, mitochondrial biogenesis, and β-oxidation markers expression. Representative Western blots for MyoD1, MEF2C, and myogenin (A)**,** MHC 1, MHC 2A, MHC 2B isoforms and total MHC (B), SDHA and CPT1-m (C) on gastrocnemius extracts. Histograms report densitometric analyses of 6-12 mice per group. [a]*P*<0.05, [b]*P*<0.001 vs SD; [c]*P*<0.05, [d]*P*<0.001 vs HFRT.

Fig. 5. **Oxidative efficiency of SDH-positive myofibers.** (A) Representative 4/20x magnification photomicrographs of SDH staining on gastrocnemius sections. Staining intensity is proportional to SDH enzymatic activity. (B) SDH enzymatic activity in whole gastrocnemius homogenates. (C) Percentage of SDH-positive on total myofibers. (D) Distribution of SDH-positive fibers among least, intermediate, and most intense SDH-staining. (E) Representative 20x magnification photomicrographs of Mitotracker staining plus immunohistochemitry for MHC 2A on gastrocnemius sections. Mitotracker staining intensity is proportional to mitochondrial membrane potential. (F) Histograms report densitometric values of 6-12 mice per group of Mitotracker fluorescence normalized for the percentage of oxidative MHC 2A myofibers. (G) Representative Western blots in total gastrocnemius extracts for sMtCK. Histogram reports densitometric analyses of 6-12 mice per group normalized for the relative tubulin content. Data are means ± standard deviation of 6-12 mice per group. [a]*P*<0.05, [b]*P*<0.001 vs SD; [c]*P*<0.05, [d]*P*<0.001 vs HFRT.

Fig. 6. **Oxidative stress markers.** (A) Representative 10x magnification photomicrographs of DHE staining on gastrocnemius sections indicating the presence of reactive oxygen species. (B) Representative Western blots for MnSOD in total gastrocnemius extracts. Histogram reports densitometric analyses of 6-12 mice per group normalized for the relative tubulin content. [b]*P*<0.001 vs SD; [c]*P*<0.05 vs HFRT.

Figure 7. Schematic illustration of the proposed effects of fructose-derived AGEs on mice skeletal muscle. AGEs endogenously formed by dietary fructose exert a multiple interference on SREBP-1c activation through increased glycation of SCAP and AGE-R1-dependent downregulation of SIRT-1. The enhanced activation of SREBP-1c activates lipogenesis and alters muscle specific proteins reprogramming, resulting in lipids accumulation, impaired oxidative metabolism and reduced muscle efficiency. The related increase in oxidative stress further contributes to AGEs generation.

Figure 1.

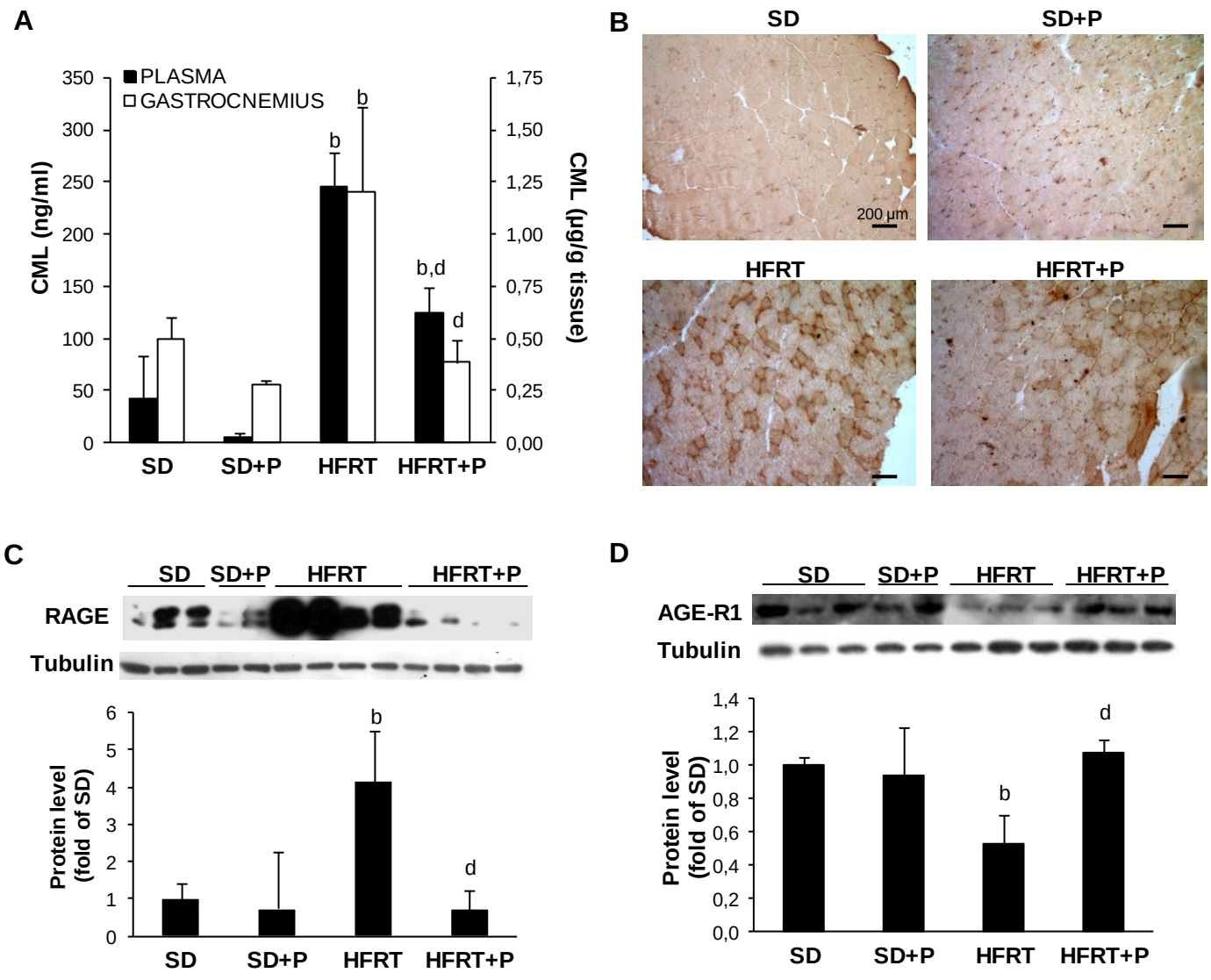
A
PLASMA
GASTROCNEMIUS
CML (ng/ml)
CML (µg/g tissue)
SD
SD+P
HFRT
HFRT+P
B
200 µm
C
RAGE
Tubulin
Protein level (fold of SD)
D
AGE-R1
Tubulin
Protein level (fold of SD)

Figure 2.

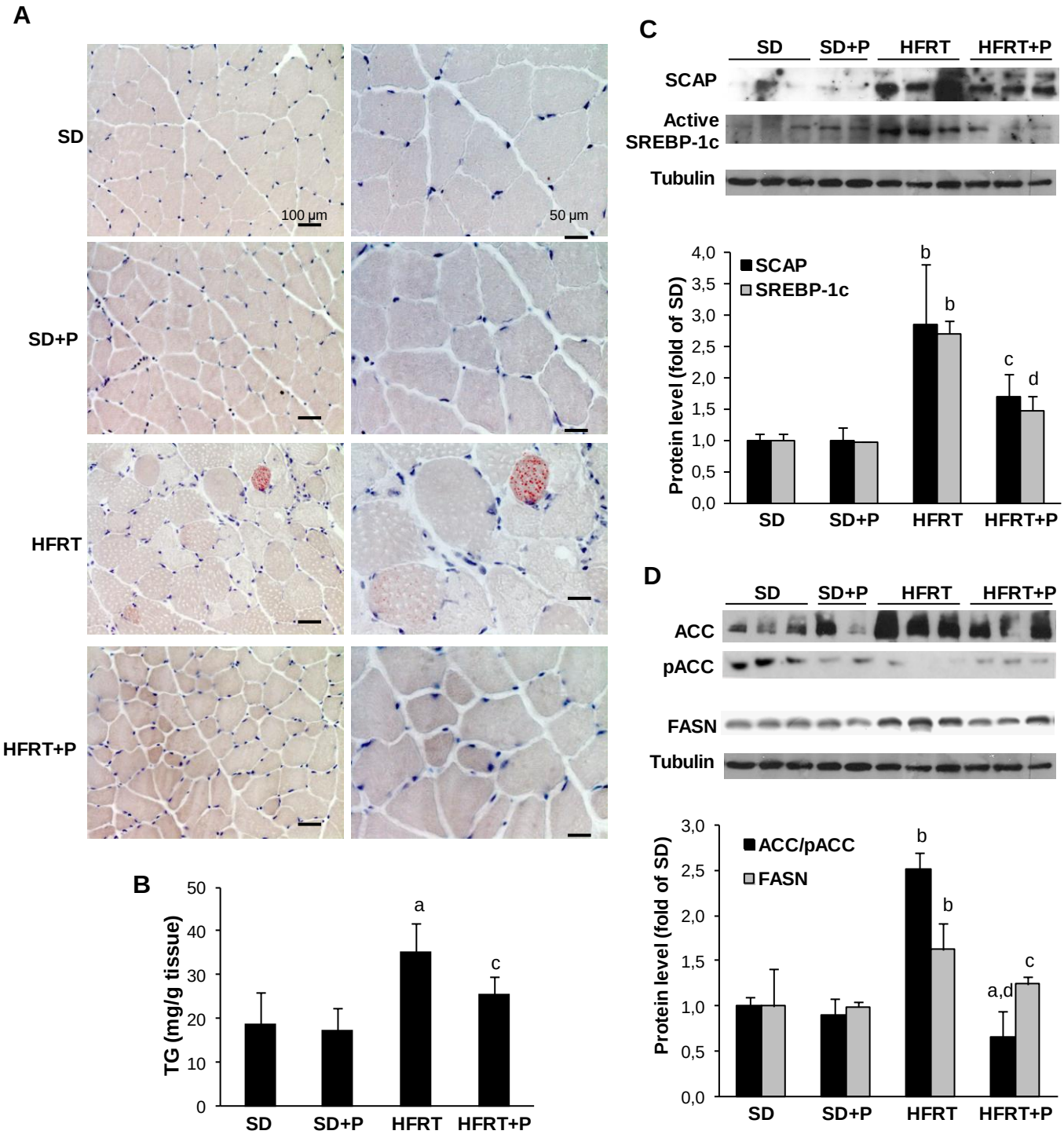
A
SD
SD+P
HFRT
HFRT+P
100 µm
50 µm
B
TG (mg/g tissue)
50
40
30
20
10
0
a
c
SD
SD+P
HFRT
HFRT+P
C
SD
SD+P
HFRT
HFRT+P
SCAP
Active SREBP-1c
Tubulin
Protein level (fold of SD)
4,0
3,5
3,0
2,5
2,0
1,5
1,0
0,5
0,0
SCAP
SREBP-1c
b
b
c
d
D
ACC
pACC
FASN
Tubulin
ACC/pACC
FASN
3,0
2,5
2,0
1,5
1,0
0,5
0,0
b
b
c
a,d

Figure 3.

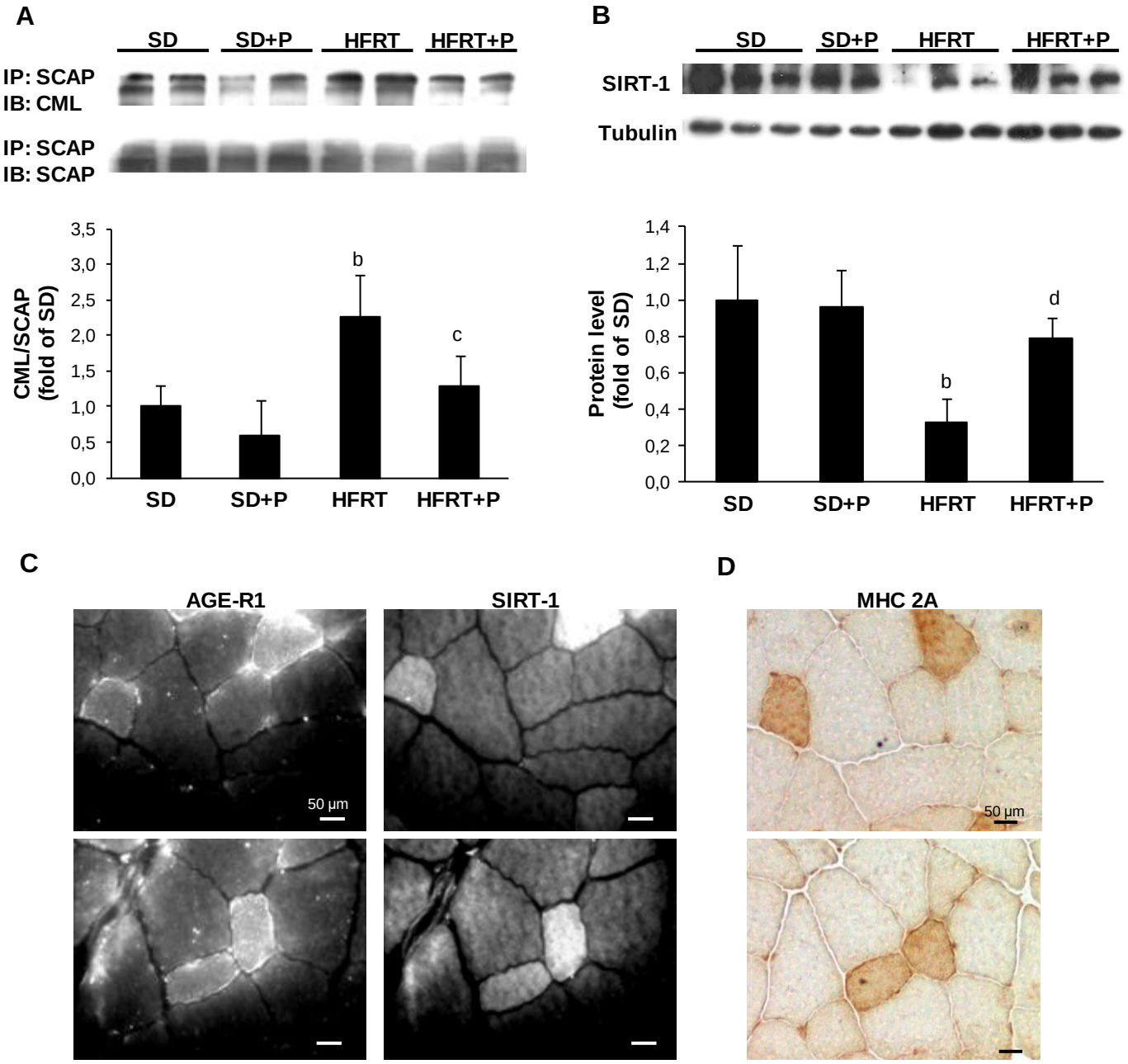
A
SD
SD+P
HFRT
HFRT+P
IP: SCAP
IB: CML
IP: SCAP
IB: SCAP
CML/SCAP (fold of SD)
3,5
3,0
2,5
2,0
1,5
1,0
0,5
0,0
b
c
SD
SD+P
HFRT
HFRT+P
B
SD
SD+P
HFRT
HFRT+P
SIRT-1
Tubulin
Protein level (fold of SD)
1,4
1,2
1,0
0,8
0,6
0,4
0,2
0,0
b
d
SD
SD+P
HFRT
HFRT+P
C
AGE-R1
SIRT-1
50 µm
D
MHC 2A
50 µm

Figure 4.

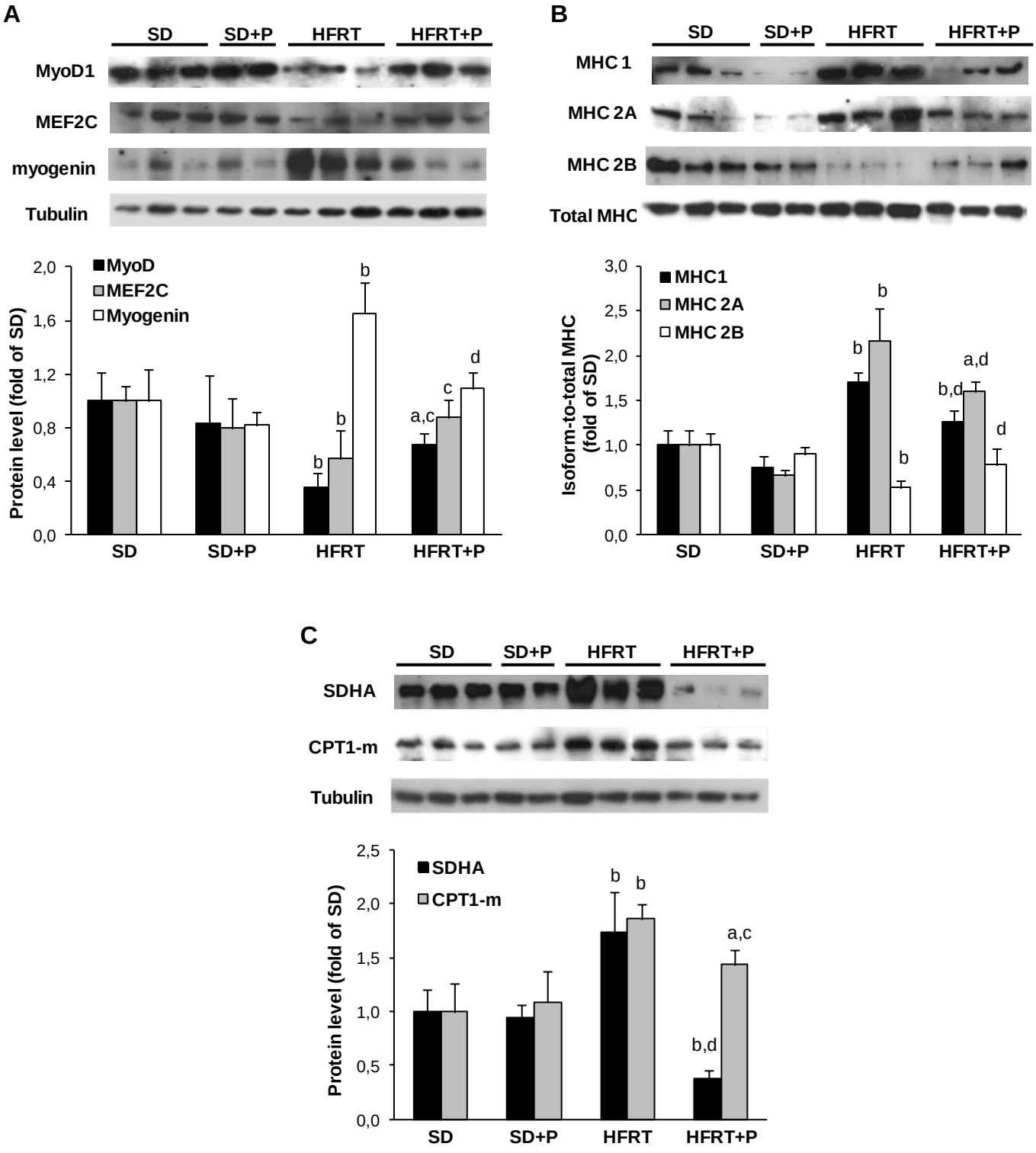
A
SD
SD+P
HFRT
HFRT+P
MyoD1
MEF2C
myogenin
Tubulin
MyoD
MEF2C
Myogenin
Protein level (fold of SD)
2,0
1,6
1,2
0,8
0,4
0,0
b
b
b
a,c
c
d
SD
SD+P
HFRT
HFRT+P
B
SD
SD+P
HFRT
HFRT+P
MHC 1
MHC 2A
MHC 2B
Total MHC
MHC1
MHC 2A
MHC 2B
Isoform-to-total MHC (fold of SD)
3,0
2,5
2,0
1,5
1,0
0,5
0,0
b
b
b
b,d
a,d
d
SD
SD+P
HFRT
HFRT+P
C
SD
SD+P
HFRT
HFRT+P
SDHA
CPT1-m
Tubulin
SDHA
CPT1-m
Protein level (fold of SD)
2,5
2,0
1,5
1,0
0,5
0,0
b
b
b,d
a,c
SD
SD+P
HFRT
HFRT+P

Figure 5.

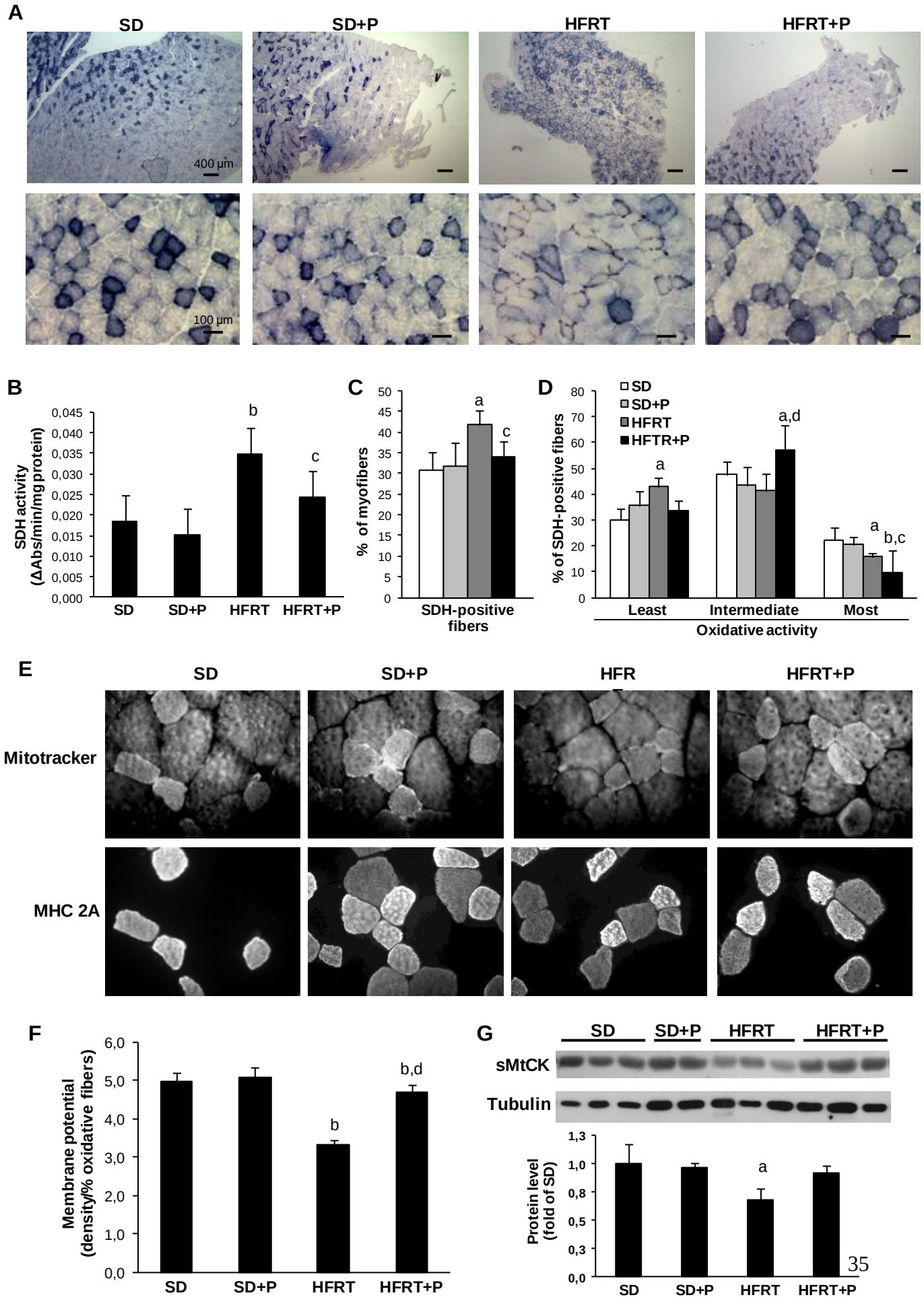
A
SD
SD+P
HFRT
HFRT+P
400 µm
100 µm
B
SDH activity (ΔAbs/min/mg protein)
0,045
0,040
0,035
0,030
0,025
0,020
0,015
0,010
0,005
0,000
b
c
SD
SD+P
HFRT
HFRT+P
C
% of myofibers
50
45
40
35
30
25
20
15
10
5
0
a
c
SDH-positive fibers
D
SD
SD+P
HFRT
HFTR+P
% of SDH-positive fibers
80
70
60
50
40
30
20
10
0
a
a,d
a
b,c
Least
Intermediate
Most
Oxidative activity
E
SD
SD+P
HFR
HFRT+P
Mitotracker
MHC 2A
F
Membrane potential (density/% oxidative fibers)
6,0
5,0
4,0
3,0
2,0
1,0
0,0
b
b,d
SD
SD+P
HFRT
HFRT+P
G
SD
SD+P
HFRT
HFRT+P
sMtCK
Tubulin
Protein level (fold of SD)
1,3
1,0
0,8
0,5
0,3
0,0
a
SD
SD+P
HFRT
HFRT+P

Figure 6.

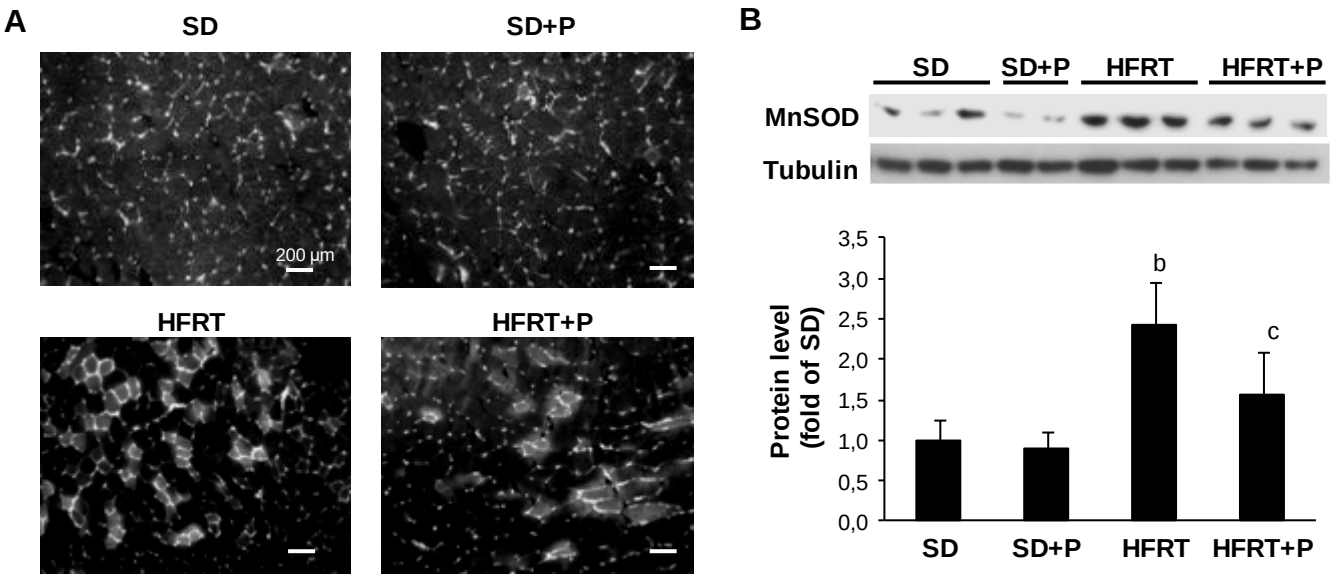
A
SD
SD+P
HFRT
HFRT+P
200 µm
B
SD
SD+P
HFRT
HFRT+P
MnSOD
Tubulin
Protein level (fold of SD)
3,5
3,0
2,5
2,0
1,5
1,0
0,5
0,0
b
c
SD
SD+P
HFRT
HFRT+P

Figure 7.

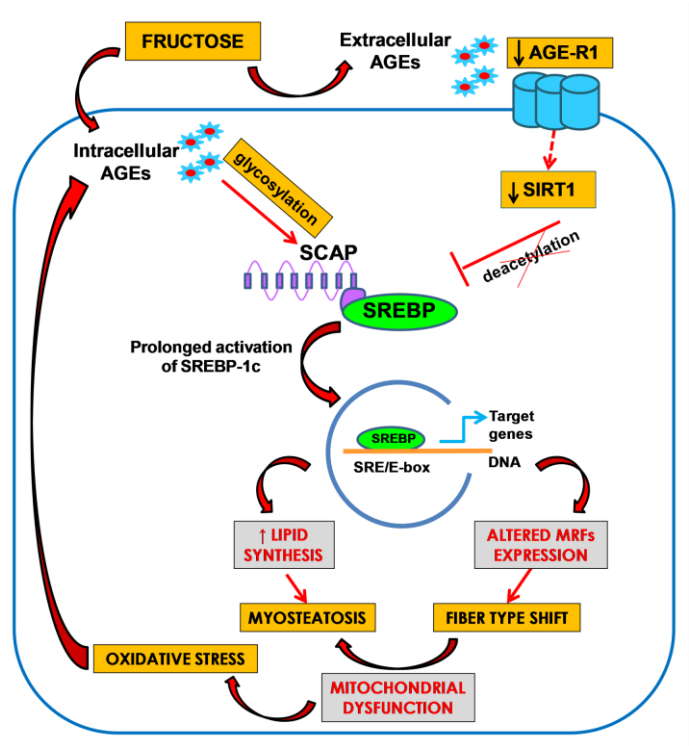
FRUCTOSE
Extracellular AGEs
↓AGE-R1
Intracellular AGEs
glycosylation
↓SIRT1
SCAP
deacetylation
SREBP
Prolonged activation of SREBP-1c
SREBP
Target genes
SRE/E-box
DNA
↑ LIPID SYNTHESIS
ALTERED MRFs EXPRESSION
MYOSTEATOSIS
FIBER TYPE SHIFT
OXIDATIVE STRESS
MITOCHONDRIAL DYSFUNCTION